

# Conformable, flexible, large-area networks of pressure and thermal sensors with organic transistor active matrixes

Takao Someya\*<sup>†</sup>, Yusaku Kato\*, Tsuyoshi Sekitani\*, Shingo Iba\*, Yoshiaki Noguchi\*, Yousuke Murase\*, Hiroshi Kawaguchi<sup>‡</sup>, and Takayasu Sakurai<sup>‡</sup>

\*Quantum-Phase Electronics Center, School of Engineering, University of Tokyo, Tokyo 113-8656, Japan; and <sup>†</sup>Center for Collaborative Research, University of Tokyo, Tokyo 153-8505, Japan

Edited by George M. Whitesides, Harvard University, Cambridge, MA, and approved July 16, 2005 (received for review March 23, 2005)

**Skin-like sensitivity, or the capability to recognize tactile information, will be an essential feature of future generations of robots, enabling them to operate in unstructured environments. Recently developed large-area pressure sensors made with organic transistors have been proposed for electronic artificial skin (E-skin) applications. These sensors are bendable down to a 2-mm radius, a size that is sufficiently small for the fabrication of human-sized robot fingers. Natural human skin, however, is far more complex than the transistor-based imitations demonstrated so far. It performs other functions, including thermal sensing. Furthermore, without conformability, the application of E-skin on three-dimensional surfaces is impossible. In this work, we have successfully developed conformable, flexible, large-area networks of thermal and pressure sensors based on an organic semiconductor. A plastic film with organic transistor-based electronic circuits is processed to form a net-shaped structure, which allows the E-skin films to be extended by 25%. The net-shaped pressure sensor matrix was attached to the surface of an egg, and pressure images were successfully obtained in this configuration. Then, a similar network of thermal sensors was developed with organic semiconductors. Next, the possible implementation of both pressure and thermal sensors on the surfaces is presented, and, by means of laminated sensor networks, the distributions of pressure and temperature are simultaneously obtained.**

electronic artificial skin | large-area sensor

Organic field-effect transistors (1–3) and their integrated circuits (4–6) have attracted considerable attention because of attributes that complement silicon-based large-scale integrations, devices that are high-performance but expensive. Organic transistors can be manufactured on plastic films at low (ambient) temperatures; therefore, they are mechanically flexible (7) and potentially inexpensive to manufacture. Two major applications drive recent studies of organic transistors. The first includes flexible displays such as paper-like displays or e-paper, in which electric inks or other media are driven by organic transistor active matrixes (8, 9). The second comprises radio frequency identification tags (10). The printable features (11–15) of organic transistors should facilitate the implementation of radio frequency identification on packages.

We have recently demonstrated another promising application: a flexible pressure sensor matrix (16, 17), in which organic transistor active matrixes are used to read out pressure data from sensors. This new pressure sensor (16, 17) could be very suitable for electronic artificial skin (E-skin), which will be an essential feature of robots, enabling them to operate in unstructured environments (18). Although the mobility of organic semiconductors is known to be about two or three orders of magnitude less than that of poly- and single-crystalline silicon, the slower speed is tolerable for most applications of large-area sensors. For E-skin in particular, the integration of pressure sensors and organic peripheral electronics allows the manufacturer to avoid

the drawbacks of organic transistors while taking advantage of their many benefits, such as mechanical flexibility, large area, low cost, and relative ease of fabrication.

Although the development of flexible pressure sensor films was an important step in endowing robots with skin sensitivity, E-skins are expected to add at least two more functionalities, namely, thermal sensing and conformability. Without conformability, it is impossible to apply E-skin to three-dimensional surfaces.

Stretchable artificial skins for humans are now commercially available, but they lack electric functionality. Indeed, various stretchable materials, such as rubber, are used in daily activities, but they have poor electrical conductivity. One of the biggest challenges in the field of electronics, particularly for E-skin applications, is the manufacture of stretchable active electronic elements and interconnects.

In this work, we demonstrate an engineering solution that employs a net-shaped structure to make flexible electronic film devices conformable to three-dimensional surfaces. Although the base films that we presently use are of polyimide and poly(ethylenephthalate), which are stiff and not inherently stretchable (in a rubber-like sense), our solution includes struts of network structures that twist with the application of tension, as may be seen in Fig. 1A. Because of this three-dimensional strut deformation, the whole network structure functions electrically with a unidirectional extension of 25%. We have implemented the pressure sensor network to the surface of an egg and have obtained pressure images in this configuration. In addition, we present data for a newly developed flexible thermal sensor network employing organic semiconductor diodes in a manner suitable for integration with the pressure sensor network. Finally, we suggest a possible implementation to attach both pressure and temperature sensor networks to a surface, and, by using two sensor networks laminated together, simultaneously measure the distribution of pressure and temperature.

## Manufacturing Process

In this section, we describe a manufacturing process for a pressure sensor network and a thermal sensor network. In the present design, both sensor networks contain their own organic transistor active matrixes for data readout. This arrangement means that each network is self-contained and electrically independent. The design of the active matrixes is exactly the same for

This paper was submitted directly (Track II) to the PNAS office.

Freely available online through the PNAS open access option.

Abbreviations: E-skin, electronic artificial skin;  $I_{DS}$ , source–drain current; PTCDI, 3,4,9,10-perylene-tetracarboxylic-diimide; parylene, polychloro-*para*-xylylene; CuPc, copper phthalocyanine;  $V_{DS}$ , source–drain voltage;  $V_{GS}$ , source–gate voltage.

<sup>†</sup>To whom correspondence should be addressed at: Quantum-Phase Electronics Center, School of Engineering, University of Tokyo, 7-3-1 Hongo, Bunkyo-ku, Engineering Building 8, Room 315, Tokyo 113-8656, Japan. E-mail: someya@ap.t.u-tokyo.ac.jp.

© 2005 by The National Academy of Sciences of the USA

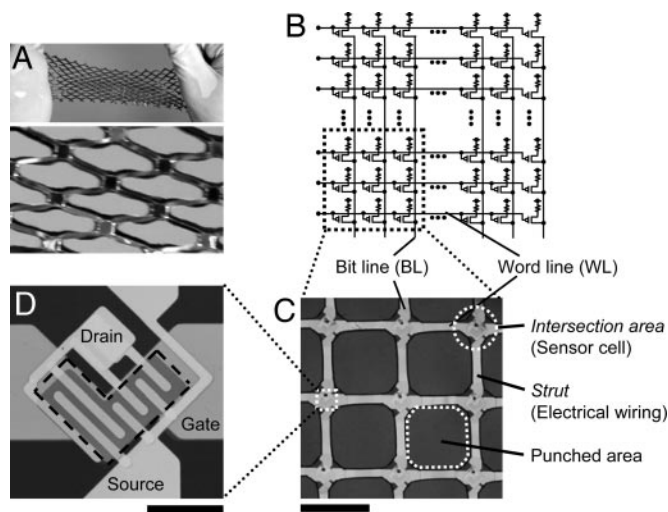


**Fig. 1.** A conformable network of pressure sensors. (A) A plastic film with organic transistors and pressure-sensitive rubber is processed mechanically to form a unique net-shaped structure, which makes a film device extendable by 25%. A magnified view of extended net-structures is also shown. (B and C) The circuit diagram of the pressure sensor network is shown (B) together with a picture of the  $3 \times 3$  sensor cells (C). A word line, denoted as WL, is connected to the gate electrodes, and a bit line, denoted as BL, is connected to the drain electrodes. The circuit diagram of the thermal sensor network can be obtained by replacing the resistances with diodes. (Scale bar: 4 mm.) (D) The optical microscopic image of an organic transistor before shaping the net or integrating it with sensors. The dotted line indicates the semiconductor channel layer. (Scale bar: 1 mm.)

both networks. The circuit diagram of the sensor film is shown in Fig. 1B; the gate electrodes of each line are connected to a word line, and drain electrodes of each line are connected to a bit line. As shown in Fig. 1C, the sensor cells are positioned at the center of “intersection areas” and are connected to each other by “struts” with electrical wirings. The magnified image of a transistor is shown in Fig. 1D. A schematic of cross-sectional structures of the two sensors is shown in Fig. 2.

**Pressure Sensor Network.** We have outlined the manufacturing process of pressure sensors in a previous article (16). First, arrays (typically  $12 \times 12$ ) of field-effect transistors with a pentacene (19–21) channel layer are manufactured on a polyimide or a poly(ethylenephthalate) film with a thickness of  $75 \mu\text{m}$ . The surface of the base film is coated with a 5-nm-thick chromium adhesion layer and a 50-nm-thick gold layer. Then, a 750-nm-

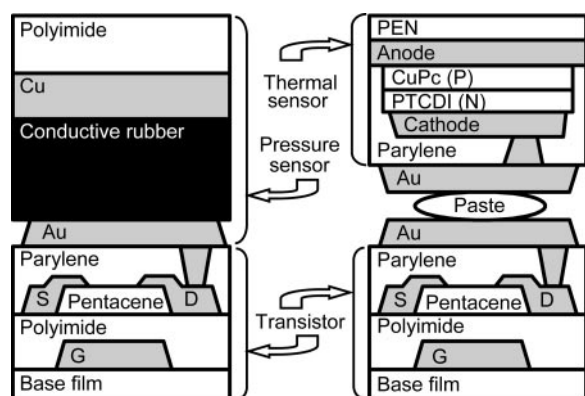


**Fig. 2.** The device structures. A cross-sectional illustration of the pressure (Left) and the thermal (Right) sensor cells with organic transistors is shown.

thick polyimide layer (22) is prepared as a gate dielectric layer. A 50-nm-thick pentacene film is deposited to form a channel layer, and a 60-nm-thick gold layer is evaporated through shadow masks to form the source and drain electrodes of the transistors. The channel length,  $L$ , and width,  $W$ , are 50 and  $1,800 \mu\text{m}$ , respectively. The periodicity is 4 mm, and the total area is  $44 \times 44 \text{ mm}^2$ . The mobility of the transistors is  $1 \text{ cm}^2/\text{Vs}$  in the saturation regime, a value that is consistent with our previous reports (16, 22). The data for a stand-alone field-effect transistor can be seen in Fig. 6, which is published as supporting information on the PNAS web site. The on/off ratio is  $10^5$  to  $10^6$  when the off current is defined as the minimum source–drain current ( $I_{\text{DS}}$ ) at a positive gate bias. As we discuss later, the on/off ratio of the transistors is sufficiently large to obtain mapping of pressure and temperature.

After the manufacturing process, the films with the organic transistors are transferred to the vacuum chamber without exposure to air, and surfaces are uniformly coated with a 2- $\mu\text{m}$ -thick polychloro-*para*-xylylene (parylene) passivation layer to form a flexible gas barrier, which helps to increase the device lifetime. Indeed, when the organic transistors with parylene were kept in air for 1 month, a change of current was <10% in the saturation regime. The parylene layer can also prevent mechanical damage to the transistors or diodes during mechanical testing. In addition, the parylene layer can suppress strains induced in transistors. To form the electronic interconnections, spots of parylene on the electrodes are removed by a  $\text{CO}_2$  laser.

The transistor film is then mechanically processed by a numerically controlled cutting plotter or drilling machine to form the net-shaped structures as shown in Fig. 1C. The use of a numerically controlled punching machine improves throughput and makes it possible to form a net shape by a roll-to-roll process. In a similar way, a pressure-sensitive rubber sheet and a copper electrode suspended by a polyimide film are cut separately to form net-shaped structures. These two films are laminated on the top of the transistor film to complete the pressure sensor network. The periodicity is 4 mm, and the width of the struts is 0.3–0.5 mm.

**Thermal Sensor Network.** The process for the thermal sensor network is as follows. Organic diodes, to be used as sheet-type thermal sensors, and whose structures are similar to electroluminescent devices (23, 24) and solar cells (25, 26), are manufactured on an indium-tin-oxide (ITO)-coated poly(ethylenephthalate) film. In a vacuum sublimation system, a 30-nm-thick p-type semiconductor of copper phthalocyanine (CuPc) and a 50-nm-thick n-type semiconductor of 3,4,9,10-perylene-tetracarboxylic-diimide (PTCDI) are deposited. Then, a 150-nm-thick gold film is deposited to form cathode electrodes having an area of  $0.19 \text{ mm}^2$ . The film with the organic diodes is coated with a 2- $\mu\text{m}$ -thick parylene layer, and the electronic interconnections are made by the method similar to that mentioned above. The diode film is also mechanically processed to form net-shaped structures. Finally, to complete the thermal sensor network, we laminated both the transistor and diode net films together with silver paste patterned by a microdispenser.

## Results

In this section, we first describe the electrical performance of the pressure sensor network and that of the thermal sensor networks separately. Then, we show how the two sensor networks can be used on the surface to simultaneously measure and map both pressure and temperature. All of the electric measurements were performed in an ambient environment with a semiconductor parameter analyzer, unless otherwise specified.

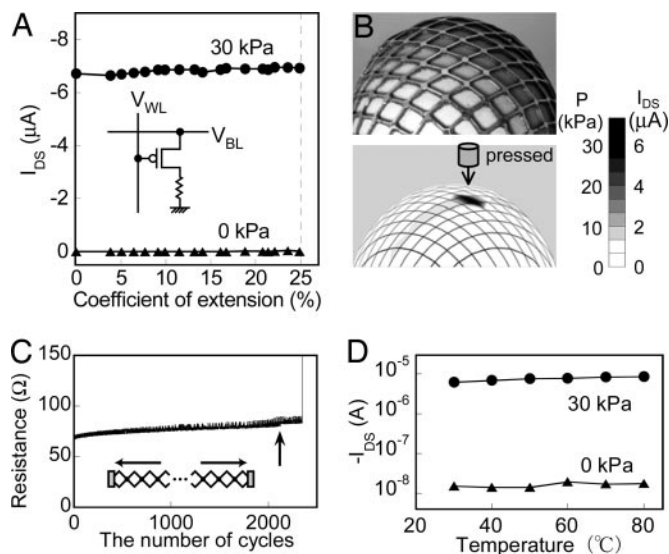


**Fig. 3.** Pressure sensor network. (A) The  $I_{DS}$  (at  $V_{DS} = V_{GS} = -40$  V) with and without application of pressure is monitored as a function of the coefficient of expansion. The dotted line represents the tension of device failure. (B) An image of pressure sensor matrix put on an egg (Upper) is shown together with a spatial distribution of pressure (Lower). The current of each sensor cell is measured by applying a voltage bias of  $V_{DS} = -20$  V and  $V_{GS} = -20$  V under the application of local pressure. (C) The results of the endurance test performed by measuring stress cycles, where each cycle comprised an extension of the film by 20% followed by the release of the stress. The resistance between both edges of the test structures is monitored as a function of the number of tension cycles. The vertical arrow represents the breaking of either one side or the other of the gold wire. The test structure is shown in the *Inset*. (D) Saturation currents  $I_{DS}$  (at  $V_{DS} = V_{GS} = -40$  V) are measured for a sensor cell of the pressure sensor network at various temperatures under the application of pressure (30 kPa) and release (0 kPa).

**Pressure Sensor Network.** One cell of the pressure sensor network was characterized. The  $I_{DS}$  of this cell integrated with organic transistors was measured at a voltage bias of  $V_{DS} = V_{GS} = -40$  V with an applied pressure of 30 kPa ( $\approx 300$  gf/cm<sup>2</sup>);  $V_{DS}$  and  $V_{GS}$  are the source–drain and source–gate voltages, respectively. Because the resistance of the rubbery sheet falls below 1 k $\Omega$  at 30 kPa, the transconductance of the integrated device is very close to that of the transistor. As a result, the current with pressure is 6.7  $\mu$ A, whereas that with no pressure is 15 nA.

With the application of tension to the pressure sensor network, which consists of many small square holes, the whole network deforms with twisted struts, as in Fig. 1A. However, we might note that, in Fig. 3A, the magnitude of the drain current  $I_{DS}$  with and without the application of pressure remains practically unchanged when the extension coefficient increases up to 25%. At extensions beyond this value, which corresponds to the application of a force of 1 N, the device does not function because of electric disconnects at the strut wirings. Such a robust performance of sensors against tension is realized in the present device because the tension induced in stiff intersection areas is considerably less than that in the twistable struts. We should note here that the conductive rubber, which is inherently stretchable, is net-shaped: under tension, the conductive rubber struts lengthen, so that the sensor performance in intersection areas is practically unaffected.

The pressure sensor network was extended and attached to the surface of an egg, as shown in Fig. 3B. To read out the data, one of the word lines is activated from low states (0 V) to high states ( $-20$  V), while all of the other word lines remain in low states (0 V). Then, current levels are read out by applying  $V_{DS} = -20$  V to each bit line. To obtain a pressure map at room temper-

ature, we repeated a similar process, activating each word line one by one. Fig. 3B Lower shows the results of the current level obtained for each sensor cell when the rubber block was positioned on two sensor cells. Only the two cells where the block is positioned were activated, although a small crosstalk was detected because of small leakage current through the gate dielectric layers of the organic transistors. When the rubber block was positioned on another pair of cells, only that pair was activated.

Compared with rubber-based stretchable conductors (27–29), the mechanical weakness of the extended networks might pose a problem. We have found that, when too much tension is applied to the device, mechanical failure always occurs around one of the bases of the struts, which then causes electric disconnections. This observation indicates that the major part of the strain is induced at the base of the struts, while it is rather small in the stiff intersection areas. In the present design, each transistor is positioned at the center of the intersection areas, and, furthermore, the area of the transistor is much smaller than that of the intersection areas to minimize the strains induced in the transistors. To examine mechanical robustness of such a design, the regions of concern are the struts used for electrical wiring rather than the intersection areas where the active device components are located. Therefore, we have prepared a simplified test structure consisting of a linear array that is part of a net structure, processed from a plastic film whose surface is uniformly coated with a 100-nm-thick gold layer. We measured the mechanical resistance of this structure by measuring stress cycles, where each cycle comprised an extension of the film by 20% followed by release of the stress. Fig. 3C shows that the device showed no significant electronic degradation even after 2,000 cycles. The mechanical resistance is, therefore, sufficient for many applications requiring a single expansion, such as a permanent application on a curved surface. A higher mechanical resistance, which might be required for applications such as the joints of arms, could be obtained if the strain near the bases of the struts is suppressed by optimizing structural parameters such as the thickness of the base films and the width of the struts. Indeed, we have found empirically that the mechanical robustness is related to the radius of the corners of punched-out squares. Thus, important issues for the future are the design and optimization of the shape of the punched-out geometric patterns.

To measure pressure and temperature simultaneously, the pressure sensor network has to be functional at the temperature of concern. We have characterized one cell of the pressure sensor networks at various temperatures. We reported earlier the details of the performance of a pressure sensor matrix at room temperature (16), and we found here that the device also works well in the temperature range from 30°C to 80°C, as shown in Fig. 3D. The performance of the present switching transistors depends on temperature, but such effects can be compensated for when the temperature is monitored simultaneously at the same position.

**Thermal Sensor Network.** Stand-alone thermal sensors are characterized in a nitrogen environment before integration with the transistors. As shown in Fig. 4A, the temperature dependence of the current is plotted as a function of  $1,000/T$ . For the purpose of comparison, we also prepared two structures with single organic semiconductor layers, a CuPc and a PTCDI layer. For a double-layer structure, the current is enhanced by a factor of 20 when the temperature is varied from 30°C to 160°C. The use of a combination of the two layers is necessary, because the temperature dependence of the devices made of only one type of layer is much smaller.

One cell of the thermal sensor network consisting of the double-layer thermal sensor array and active matrix was characterized at temperatures between 30°C and 80°C, and the

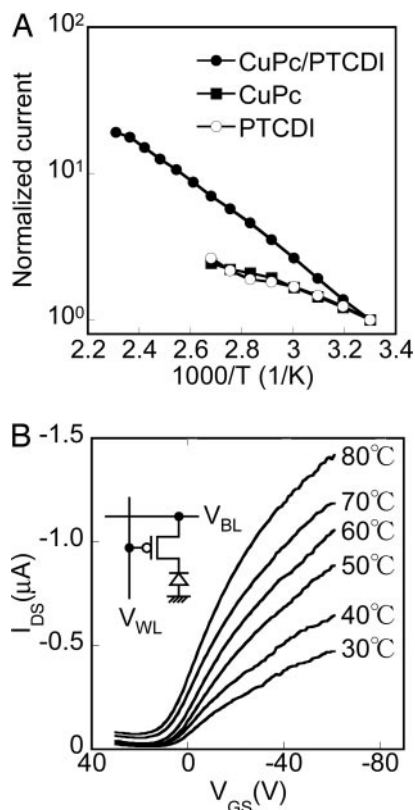


**Fig. 4.** Thermal sensor network. (A) Temperature dependence of current is measured under voltage bias of 2 V, and data normalized by current at room temperature are plotted as a function of  $1,000/T$  for three samples: stand-alone thermal sensors, denoted by solid circles, consisting of double organic semiconductors (30-nm-thick CuPc and 50-nm-thick PTCDI), and single organic semiconductor (80-nm-thick CuPc or 80-nm-thick PTCDI, denoted by solid squares and open circles, respectively) sandwiching between ITO and Au electrodes. (B) One cell of the thermal sensor network devices consisting of the diode-based thermal sensors and transistors is characterized at various temperatures from 30°C to 80°C.

results are shown in Fig. 4B. Because the measurement was performed under an ambient environment, the performance was slightly degraded because of oxygen and/or moisture exposure during measurement; the temperature dependence obtained was smaller than the measurement obtained under a nitrogen environment. Thus, a further optimization of the parylene passivation layer, particularly with regard to the thickness of the parylene and the deposition conditions, is required to minimize the degradation associated with exposure to oxygen and/or moisture. We have performed 10 heat-cycle tests between 30°C and 100°C and found that the current distribution was less than  $\pm 10\%$ .

To map temperatures with the active matrix, it is very important that the thermal sensors themselves respond strongly to temperature while the change of performance of switching transistors remains small. Indeed, as mentioned above, the organic diode-based sensors exhibit a current enhancement by a factor of 20 when the temperature is varied from 30°C to 160°C; under the same conditions, the current of the organic transistors changed only by a factor of 3.

**Temperature and Pressure Mapping.** The final step is the implementation of both the thermal and pressure sensor films on the target surface. In a practical production scheme, this process can be carried out by successively laminating the sensor films one by one on the surface, so that the thermal sensors and pressure

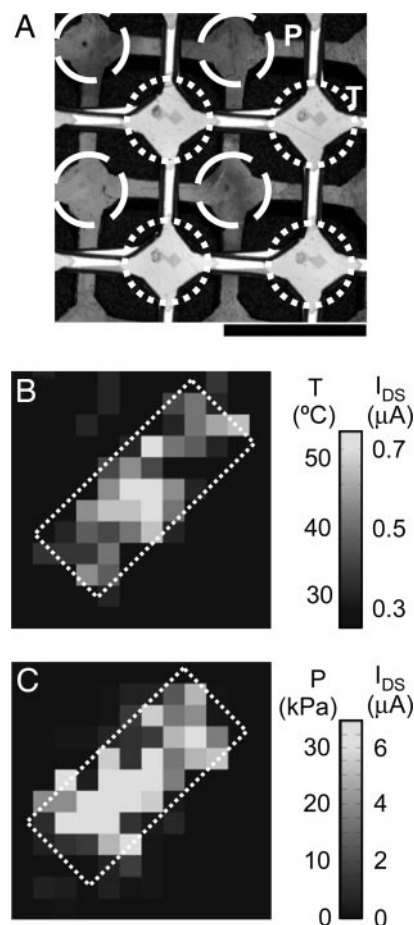


**Fig. 5.** Integration of pressure and thermal sensor networks. (A) A possible implementation of thermal and pressure sensor films. The pressure and thermal sensors are represented by P and T, respectively. (Scale bar: 4 mm.) (B) The spatial distribution of temperature that is converted from the temperature-dependent current in the thermal sensor network. A copper block ( $15 \times 37$  mm<sup>2</sup>) whose temperature is maintained at 50°C is positioned diagonally (indicated by the dotted line). The sensing area is  $44 \times 44$  mm<sup>2</sup>. (C) Simultaneously, the spatial distribution of pressure is measured with the pressure sensor network.

sensors form checkerboard patterns, as shown in Fig. 5A. Such a manufacturing process is possible because each sensor film has its own active matrix and is electrically independent. Although the present network device can be applied to a curved surface, in the following mapping experiment we mounted both the thermal and pressure sensor networks on a flat board to achieve a good thermal contact over a wide area.

In the described configuration with two sensor networks, measurements of temperature and pressure mapping were performed simultaneously. The spatial distribution of the temperature-dependent current was measured by applying individually to each sensor cell a voltage  $V_{DS} = -2$  V for each bit line and  $V_{GS} = -40$  V for each word line; simultaneously, the spatial distribution of pressure was measured by applying individually to each sensor cell a voltage  $V_{DS} = -20$  V for each bit line and  $V_{GS} = -20$  V for each word line. A copper block whose temperature was maintained at 50°C was positioned diagonally. The measured temperature and pressure distributions are shown in Fig. 5B and C, respectively, with the dotted-line rectangle indicating the area of the copper block. In both figures, sensor cells, on which the block was positioned, were activated. Both figures look similar because the same positions are pressed simultaneously; however,

small discrepancies between two figures should be ascribed to nonuniformity of pressure and temperature applied over a wide area.

## Discussion

The most important factor for obtaining accurate spatial distributions of pressure and temperature is a high yield of the sensor cells, rather than a high sensitivity for each cell. By using state-of-the-art manufacturing technology for the organic transistors, which has been reported in detail elsewhere (16), we were able to fabricate an array in which all  $12 \times 12$  transistors and diodes are functional, even though we often observed a fairly large variation of the performance of individual transistors. This last disadvantage may be problematic for applications such as flexible displays (8, 9) and radio frequency identification tags (10). However, even though this performance variation might degrade the accuracy of the temperature readout, it could easily be compensated for by an adequate calibration procedure as is usually carried out for area sensors such as image scanners and touch panels. A possible calibration procedure is as follows: scanning all sensor cells at 30°C and 80°C, scanning images, and then calibrating the images by interpolating data between 30°C and 80°C.

It is very important to obtain a large on/off ratio of the transistors. In particular, the off current of the transistors should be small even at a high temperature to use the transistors as electronic switches to read out accurately the current from the diodes. We have obtained on/off ratios that are relatively insensitive to temperature and exceed  $10^5$  even at 80°C.

There are many benefits to a net-shaped film device apart from conformability. First, a good isolation of each sensor leads to more accurate sensing. In particular, for an accurate measurement of temperature, it is very important to suppress thermal perturbation due to heat flow from neighboring regions. In a net-shape structure, such a thermal flow can be minimized by reducing the width of the struts. Second, the present net-shaped structures make possible the inclusion of various kinds of sensors on the film surfaces, a factor that is very important to perform accurate measurements of temperature and pressure. The present scheme simplifies the fabrication process, because various types of sensors can be prepared separately and laminated together in the last fabrication steps. The thickness of one of the sensor films causes small steps, which may degrade the accuracy of the sensing measurements. The step height of the present thermal sensor film is  $\approx 200 \mu\text{m}$ , but it can be reduced by one order of magnitude. Indeed, our group and another research group have manufactured organic transistors active matrixes on 10- to 25- $\mu\text{m}$ -thick plastic films (30). Thus, it will be possible in the near future to make an electronic skin that has functions that human skin lacks by integrating various sensors not only for pressure and temperature, but also for light, humidity, strain, sound, or ultrasonic.

We thank Profs. Y. Arakawa, H. Sakaki, M. Gonokami, and T. Kobayashi for fruitful discussions and Dr. J. B. Héroux for a critical reading of the manuscript. This study was partially supported by the Information Technology Program and TOKUTEI (15073204) of the Ministry of Education, Culture, Sports, Science, and Technology of Japan and by the New Energy and Industrial Technology Development Organization.

1. Tsumura, A., Koezuka, H. & Ando, T. (1986) *Appl. Phys. Lett.* **49**, 1210–1212.
2. Dimitrakopoulos, C. D. & Malenfant, P. R. L. (2002) *Adv. Mater.* **14**, 99–117.
3. Dodabalapur, A., Torsi, L. & Katz, H. E. (1995) *Science* **268**, 270–271.
4. Crone, B., Dodabalapur, A., Lin, Y.-Y., Filas, R. W., Bao, Z., LaDuca, A., Sarpeshkar, R., Katz, H. E. & Li, W. (2000) *Nature* **403**, 521–523.
5. Drury, C. J., Mutsaers, C. M. J., Hart, C. M., Matters, M. & Leeuw, D. M. (1998) *Appl. Phys. Lett.* **73**, 108–110.
6. Gelinck, G. H., Geuns, T. C. T. & Leeuw, D. M. (2000) *Appl. Phys. Lett.* **77**, 1487–1489.
7. Sekitani, T., Kato, Y., Iba, S., Shinaoka, H., Someya, T., Sakurai, T. & Takagi, S. (2005) *Appl. Phys. Lett.* **86**, 073511.
8. Rogers, J. A., Bao, Z., Baldwin, K., Dodabalapur, A., Crone, B., Raju, V. R., Kuck, V., Katz, H., Amundson, K., Ewing, J. & Drzaic, P. (2001) *Proc. Natl. Acad. Sci. USA* **98**, 4835–4840.
9. Gelinck, G. H., Huitema, H. E. A., Veenendaal, E., Cantatore, E., Schrijnemakers, L., Putten, J., Geuns, T. C. T., Beenhakkers, M., Giesbers, J. B., Huisman, B.-H., et al. (2004) *Nat. Mater.* **3**, 106–110.
10. Baude, P. F., Ender, D. A., Haase, M. A., Kelley, T. W., Muires, D. V. & Theiss, S. D. (2003) *Appl. Phys. Lett.* **82**, 3964–3966.
11. Sirringhaus, H., Kawase, T., Friend, R. H., Shimoda, T., Inbasekaran, M., Wu, W. & Woo, E. P. (2000) *Science* **290**, 2123–2126.
12. Loo, Y.-L., Someya, T., Baldwin, K. W., Bao, Z., Ho, P., Dodabalapur, A., Katz, H. E. & Rogers, J. A. (2002) *Proc. Natl. Acad. Sci. USA* **99**, 10252–10256.
13. Stutzmann, N., Friend, R. H. & Sirringhaus, H. (2003) *Science* **299**, 1881–1884.
14. Katz, H. E., Lovinger, A. J., Johnson, J., Kloc, C., Siegrist, T., Li, W., Lin, Y.-Y. & Dodabalapur, A. (2000) *Nature* **404**, 478–481.
15. Yang, Y. & Heeger, A. J. (1994) *Nature* **372**, 344–346.
16. Someya, T., Sekitani, T., Iba, S., Kato, Y., Kawaguchi, H. & Sakurai, T. (2004) *Proc. Natl. Acad. Sci. USA* **101**, 9966–9970.
17. Someya, T., Kawaguchi, H. & Sakurai, T. (2004) in *International Solid-State Circuits Conference Digest of Technical Papers* (IEEE Solid-State Circuits Soc., Piscataway, NJ), pp. 288–289.
18. Nicholls, H. R. & Lee, M. H. (1989) *Int. J. Robotics Res.* **8**, 3–30.
19. Klauk, H., Halik, M., Zschieschang, U., Schmid, G., Radlik, W. & Weber, W. (2002) *J. Appl. Phys.* **92**, 5259–5263.
20. Klauk, H., Gundlach, D. J. & Jackson, T. N. (1999) *IEEE Electron Device Lett.* **20**, 289–291.
21. Dimitrakopoulos, C. D., Purushothaman, S., Kymissis, J., Callegari, A. & Shaw, J. M. (1999) *Science* **283**, 822–824.
22. Kato, Y., Iba, S., Teramoto, R., Sekitani, T., Someya, T., Kawaguchi, H. & Sakurai, T. (2004) *Appl. Phys. Lett.* **84**, 3789–3791.
23. Burroughes, J. H., Jones, C. A. & Friend, R. H. (1988) *Nature* **335**, 137–141.
24. Sirringhaus, H., Tessler, N. & Friend, R. H. (1998) *Science* **280**, 1741–1744.
25. Peumans, P., Yakimov, A. & Forrest, S. R. (2003) *J. Appl. Phys.* **93**, 3693–3723.
26. Tang, C. W. (1986) *Appl. Phys. Lett.* **48**, 183–185.
27. Lacour, S. P., Wagner, S., Huang, Z. Y. & Suo, Z. (2003) *Appl. Phys. Lett.* **82**, 2404–2406.
28. Lacour, S. P., Jones, J., Suo, Z. & Wagner, S. (2004) *IEEE Electron Device Lett.* **25**, 179–181.
29. Jones, J., Lacour, S. P., Wagner, S. & Suo, Z. (2004) *J. Vac. Sci. Technol. A* **22**, 1723–1725.
30. Gelinck, G. H., Huitema, H. E. A., van Mil, M., van Veenendaal, E., van Lieshout, P. J. G. & Touwslager, F. J. (2005) in *Technical Digest of the Society for Information Display* (Soc. for Information Display, San Jose, CA), pp. 6–9.